Supporting Information

Quantification of Active Site Density and Turnover Frequency: From Single-Atom Metal to Nanoparticle Electrocatalysts

Geunsu Bae,[1,†] Haesol Kim,[1,†] Hansol Choi,[1] Pyeonghwa Jeong,[2] Dong Hyun Kim,[1] Han Chang Kwon,[3] Kug-Seung Lee,[4] Minkee Choi,[3] Hyung-Suk Oh,[5,6] Frédéric Jaouen,[7,]* and Chang Hyuck Choi[1,]*

[1]School of Materials Science and Engineering, Gwangju Institute of Science and Technology, Gwangju 61005, Republic of Korea.

[2]Department of Chemistry, Duke University, Durham, North Carolina 27708, United States.

[3]Department of Chemical and Biomolecular Engineering, Korea Advanced Institute of Science and Technology, Daejeon 34141, Republic of Korea.

[4]Beamline Department, Pohang Accelerator Laboratory, Pohang University of Science and Technology, Pohang 37673, Republic of Korea.

[5]Clean Energy Research Center, Korea Institute of Science and Technology, Seoul 02792, Republic of Korea.

[6]KHU-KIST Department of Conversing Science and Technology, Kyung Hee University, Seoul 02447, Republic of Korea.

[7]ICGM, Univ. Montpellier, CNRS, ENSCM, Montpellier, France.

†These authors contributed equally to this work.

*Corresponding Authors: chchoi@gist.ac.kr (C.H.C.) and frederic.jaouen@umontpellier.fr (F. J.)

Supplementary Note 1

Physicochemical characteristics of Fe$_{0.5}$NC: Fe$_{0.5}$NC contained Fe content of *ca.* 1.5 wt% as confirmed by ICP-AES (Table S1). XRD and Raman spectroscopy confirmed the successful carbonization of the precursor mixture during pyrolysis (Figure S1a and b). XPS revealed the functionalization of the carbon support with N moieties, which could act as anchoring sites for the stabilization of the isolated Fe ions (Figure S1c). The extended X-ray absorption fine structure (EXAFS) spectrum showed the presence of a strong Fe-N(O) interaction, without Fe-Fe interaction, similar to that for molecular Fe-phthalocyanine (FePc; Figure S1d). Furthermore, its ^{57}Fe Mössbauer spectrum could be fitted with two doublets, D1 and D2 (Figure S1e and Table S2), which were assigned to the Fe-N$_x$ moieties.[1] The absence of the singlet and sextet signals in the fitting of the ^{57}Fe Mössbauer spectrum as well as evidence for no Fe-Fe interaction in the EXAFS spectrum supported the predominant presence of the isolated Fe-N$_x$ moieties without discernible amounts of Fe clusters in Fe$_{0.5}$NC. The atomic dispersion of Fe species could be further visualized by HAADF-STEM analyses (Figure S1f).

Supplementary Note 2

ORR activity measurement protocol for *in situ* SD quantification using cyanide probe: The typical ORR measurement protocol in a half-cell system includes CV or LSV in the potential range of 0.05–1.05 V$_{RHE}$ at a scan rate of 5–100 mV s^{-1}.[2] Unfortunately, this conventional protocol introduced non-negligible deviations in the estimated j (kinetic current density (j_k) and diffusion-limited current density (j_d) as well) and consequent SD values in repeated analyses (Figure S8). This deviations possibly resulted from 1) the errors in the subtraction of non-Faradaic capacitive j and/or 2) undesirable reaction between the H$_2$O$_2$ byproduct and adsorbed cyanide.[3,4] Note that *ca.* 10% deviation in the estimated SD value for Fe$_{0.5}$NC could be obtained with only small changes in the j value of 5 µA cm^{-2} at 0.85 V$_{RHE}$. Therefore, several ORR measurement conditions for reliable SD quantification were investigated, and an LSV from 0.70 to 1.05 V$_{RHE}$ with a slow scan rate of 1 mV s^{-1} was finally employed. This afforded good reproducibility of the ORR polarization curves for the poisoned catalysts with minimized interference of the non-Faradaic j and H$_2$O$_2$ (E^0 = 0.69 V$_{RHE}$ for O$_2$/H$_2$O$_2$). The electrocatalytic activity of Fe$_{0.5}$NC was then compared at 0.85 V$_{RHE}$, where the contribution of j_d to j was almost negligible and j was almost identical to j_k (Figure S9). This ORR activity measurement protocol yielded a deviation of only ± 3% in the estimated SD values.

Supplementary Note 3

Non-site-specific adsorption of cyanide on Fe-N$_x$ moieties: As the ^{57}Fe Mössbauer spectrum of Fe$_{0.5}$NC exhibits two doublets D1 and D2 (Figure S1e and Table S2), the ORR activity of Fe$_{0.5}$NC can be expressed in terms of the intrinsic TOF and absolute amount (*i.e.*, SD) of D1 and D2 species using the following equation:

$$J \ [\text{A g}^{-1}] = J_{D1} + J_{D2} = \left({TOF_{D1} \times SD_{D1} \times F}/{N_A} \right) + \left({TOF_{D2} \times SD_{D2} \times F}/{N_A} \right) \tag{Eq. S1}$$

where J is the catalytic mass activity at a given potential, N_A is the Avogadro constant, and F is the Faraday constant. Similarly, the ORR activity of the cyanide-poisoned catalyst (J') and the decrease in the catalytic activity (ΔJ) can be expressed by the following equations:

$$J' \ [\text{A g}^{-1}] = J'_{D1} + J'_{D2} = \{J_{D1} \times (1 - \alpha_{D1})\} + \{J_{D2} \times (1 - \alpha_{D2})\} \tag{Eq. S2}$$

$$\Delta J \ [\text{A g}^{-1}] = J - J' = (J_{D1} \times \alpha_{D1}) + (J_{D2} \times \alpha_{D2}) \tag{Eq. S3}$$

where α is the fraction of poisoned sites to the total number of sites of each species. Assuming that D1 and D2 species have completely different binding affinities to cyanide, cyanide poisoning on Fe-N$_x$ moieties does not occur randomly, but is more selective to specific Fe species (*i.e.*, $\alpha_{D1} \neq \alpha_{D2}$). Therefore, if the extent of the irreversible cyanide adsorption varies (by controlling the potential applied or initial cyanide concentration) during the *in situ* SD quantification protocol, the changes in ΔJ would be more dominantly affected by the active Fe species with a relatively stronger cyanide binding affinity than the species with a weak binding affinity. This can lead to substantial changes in the SD values estimated by Eqs. 1 and 2 (noted in the main article), which are derived with the assumption of non-site-specific adsorption of cyanide (*i.e.*, $\alpha_{D1} = \alpha_{D2}$). However, in practice, the *in situ* SD quantification afforded an almost identical SD value of $(3.38 \pm 0.48) \times 10^{19}$ sites g^{-1} for Fe$_{0.5}$NC. No significant deviations in the SD value were observed, regardless of the different extents of irreversibly adsorbed cyanide, thereby corroborating the assumption of the non-site-specific adsorption of cyanide. Moreover, with this assumption (*i.e.*, random cyanide poisoning on surface Fe-N$_x$ sites) and undistinguishable contribution of each site in the measured J value, we can safely average the TOFs of different sites despite their own intrinsic TOF (Eq. S4). Although estimation of each TOF of active sites having different local chemical natures is hardly achieved, we note that such a drawback is also found in the previously reported CO chemisorption and the NO$_2^-$-stripping methods for Fe-N-C catalysts,[5,6] and in the H$_{UPD}$ and CO-stripping methods for Pt nanoparticle catalysts.[7,8]

$$J \ [\text{A g}^{-1}] = \left({TOF_{avg.} \times F}/{N_A} \right) \times (SD_{D1} + SD_{D2}) \tag{Eq. S4}$$

Interestingly, the local position and chemical nature of the D1 and D2 sites of $Fe_{0.5}NC$ were recently investigated. Mineva *et al.* reported the oxidation and electron-spin states of D1 and D2 sites with their local positions *via* bridged ^{57}Fe Mössbauer spectroscopy and DFT calculations,[1] suggesting that D1 corresponded to the surface-exposed ferric moieties and D2 to the O_2-inaccessible or surface-exposed with weak O_2 binding ferrous moieties. In addition, the *in situ* Mössbauer spectra of $Fe_{0.5}NC$ during fuel cell operation revealed a complete switch of the D1 signal but an almost unaltered D2 signal.[9] If their prediction is true, *i.e.*, the inaccessibility of the D2 site, only D1 site can be considered in Eqs. S1–4 without any contribution of the D2 site. This also supports the validity of Eqs. 1 and 2 (noted in the main article) owing to the non-site-specific adsorption of cyanide on a single D1 site.

Supplementary Note 4

Different cyanide adsorption modes of heterogeneous Pt sites with different surface coverages: As bulk Pt typically contains heterogeneous surface sites (*e.g.*, different facet, edge, etc.) and the cyanide adsorption modes and surface coverages are not identical,[10] their comprehensive contributions should be considered to more accurately calculate the SD values. Hence, the SD value of Pt nanoparticles was calculated using the following equation, which was slightly modified from the equation used for the SACs:

$$\text{SD [sites g}^{-1}] = [(\Delta C_{CN^-}^{\text{electrolyte}} \times V \times N_A / m_{\text{cat}})/(\Delta j / j_{\text{pristine}})] \times \sum \frac{(\varphi/100)}{\theta} \qquad \text{(Eq. S5)}$$

where φ and θ are the surface composition (%) and surface coverage (*i.e.*, CN$^-$/Pt) of different Pt sites, respectively. With further deconvolution of the individual φ and θ values of heterogeneous Pt sites, a more thorough SD quantification of Pt nanoparticles can be performed. In the literature, Shao *et al.* reported the particle size dependence of φ value of the Pt nanoparticles based on the DFT calculations on the truncated octahedral models,[11] where an increase in the particle size resulted in an increase in the φ values for Pt(111) and Pt(100) but a decrease in that for the Pt edge sites (Figure S25a). Based on the theoretical φ values, the U values of the Pt samples could be roughly estimated. Here, the θ value of each Pt site was assumed to be 0.5 for Pt(111) according to the literature,[12] and 1.0 for Pt(100) and edge. This calculation resulted in a U value of 52% for 2.5-nm Pt nanoparticle, which decreased to 45, 34, and 18% when increasing the particle size to 2.9, 3.8, and 4.5 nm, respectively (Figure S25b). Compared to those obtained by a simple assumption of $\theta = 0.5$ for Pt(111) (*i.e.*, 67, 56, 41, and 22% for 2.5, 2.9, 3.8, and 4.5 nm, respectively), the consideration of φ and θ for the heterogeneous Pt sites effectively reduced the deviations from the U values obtained by ECSA$_{CO}$ (*i.e.*, 53, 39, 21, and 14%, respectively). Despite the non-negligible difference between the U values estimated using different probe molecules (*i.e.*, cyanide and CO), the above examples suggest that the *in situ* quantification method with cyanide probe can potentially be used for the accurate SD quantification of Pt nanoparticles if accurate φ and θ of each site are determined.

Supplementary Figures
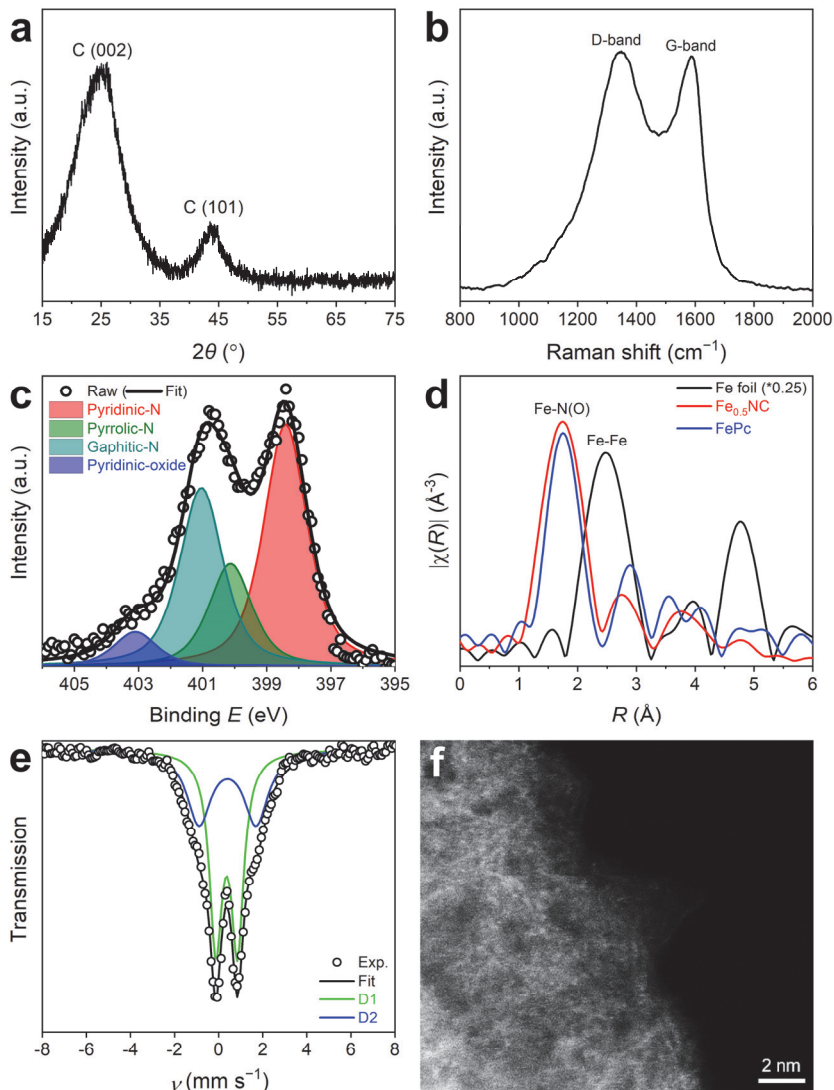
**Figure S1**. Physicochemical characterization of $Fe_{0.5}NC$. (a) XRD pattern and (b) Raman spectrum of $Fe_{0.5}NC$.

Two main peaks of graphite in the XRD pattern and D-/G-band signals in the Raman spectrum indicate the

successful carbonization of the $Fe_{0.5}NC$ precursor mixture during pyrolysis. (c) XPS-N_{1s} spectrum of $Fe_{0.5}NC$.

The peaks are deconvoluted with four N-components: pyridinic-N (398.5 eV), pyrrolic-N (400.1 eV), graphitic-

N (401.1 eV), and pyridinic-oxide (403.2 eV).[13] (d) k^2-weighted Fourier transforms of Fe K-edge EXAFS of

$Fe_{0.5}NC$, FePc, and Fe foil. The EXAFS spectrum of $Fe_{0.5}NC$ shows a strong backscattering signal of Fe-N (or

Fe-O) bonds, which is analogous to that of FePc. (e) ^{57}Fe Mössbauer spectrum of $Fe_{0.5}NC$. Two doublets (*i.e.*, D1

and D2, indicating ferric and ferrous $Fe-N_x$ moieties of high and low/medium spins, respectively) are observed

without the signals for bulk Fe species (*e.g.*, α/γ-Fe or Fe carbide).[1] (f) HAADF-STEM image of $Fe_{0.5}NC$ (scale

bar = 2 nm).
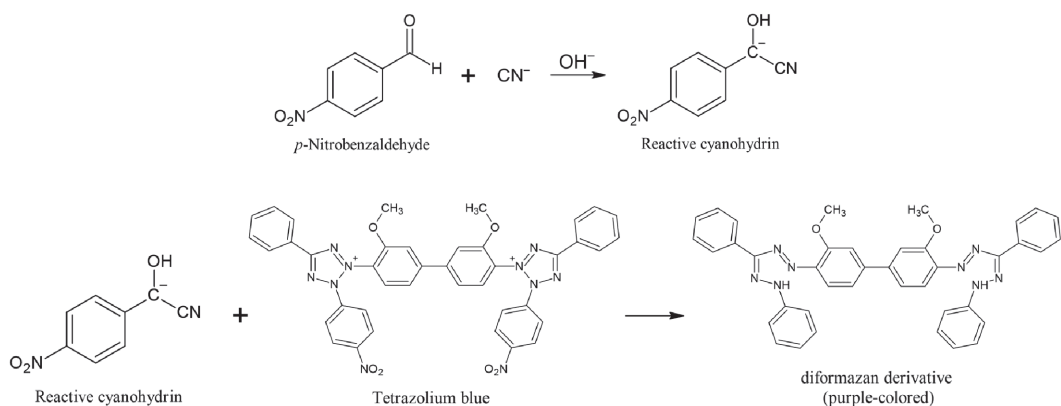
Figure S2. Chemical reactions in the spectrophotometric titration of cyanide. This method is based on the cascade catalytic reaction of cyanide with *p*-nitrobenzaldehyde and subsequently tetrazolium blue, ultimately leading to the conversion of tetrazolium blue into a purple-colored diformazan derivative.[14,15]
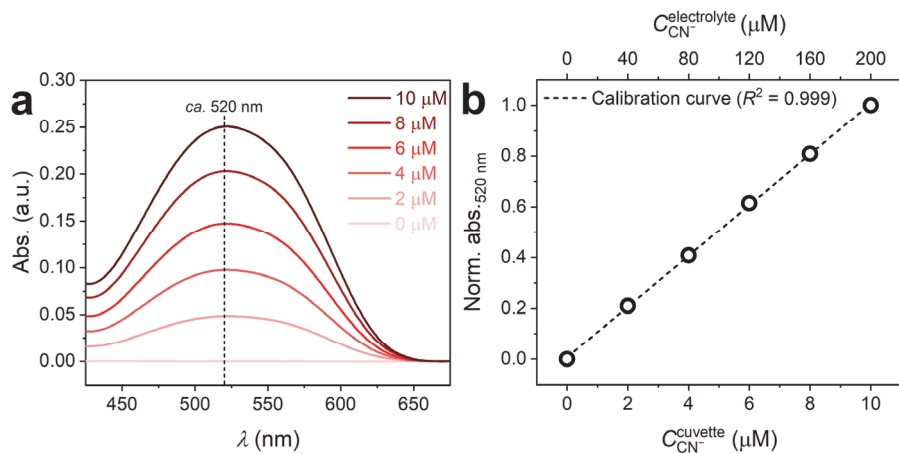
Figure S3. Spectrophotometric titration of cyanide using an UV-vis spectrophotometer. (a) UV-vis spectra of electrolyte samples. The electrolyte samples ($C_{CN^-}^{electrolyte}$ = 0–200 μM) were diluted to one-twentieth concentrations ($C_{CN^-}^{cuvette}$ = 0–10 μM) with deionized water before the measurements. The maximum absorbance is observed at *ca.* 520 nm. (b) Normalized absorbance of the electrolyte samples at 520 nm as a function of cyanide concentration. This calibration curve is obtained for each measurement to calculate $\Delta C_{CN^-}^{electrolyte}$ before and after the *in situ* SD quantification.
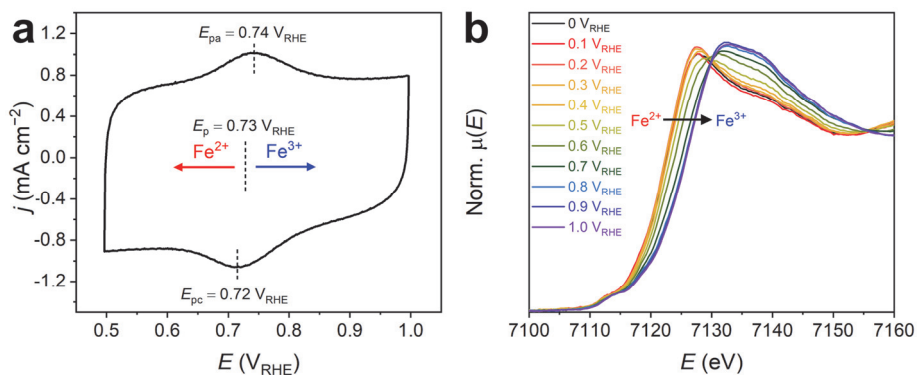
Figure S4. Fe^{2+}/Fe^{3+} redox couple of $Fe_{0.5}NC$ collected in Ar-saturated 0.1 M $HClO_4$ electrolyte. (a) A CV response of $Fe_{0.5}NC$, showing Fe^{2+}/Fe^{3+} redox couple at $E_p = 0.73$ V_{RHE} ($E_{pa} = 0.74$ V_{RHE} and $E_{pc} = 0.72$ V_{RHE}). (b) Fe K-edge *in situ* XANES spectra of $Fe_{0.5}NC$ as a function of the applied potential, showing that the population of Fe^{3+} species increases with an increase in potential.
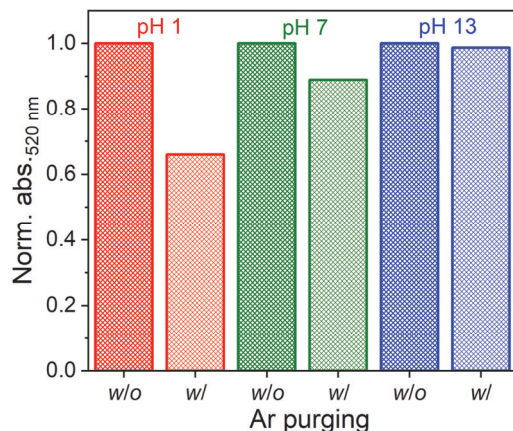
Figure S5. Effects of Ar purging in the third step of the *in situ* SD quantification protocol. UV-vis measurement on the aliquots of diluted electrolytes after cyanide introduction at different electrolyte pH values (*i.e.,* 1, 7, and 13). Cyanide poisoning experiments were conducted using the original protocol (*i.e.*, E_{third} = 1.0 V$_{RHE}$ and $C_{CN^-}^{electrolyte}$ = 200 μM), but no catalyst powders were introduced in the electrolyte. During the third step of the protocol (*i.e.*, cyanide introduction), the electrolyte was either purged with Ar gas or completely closed without Ar purging. The results show that Ar purging removes the cyanide (or HCN) dissolved in the electrolyte and this phenomenon is magnified with a decrease in the electrolyte pH. Therefore, for the accurate measurement of SD, the electrolyte compartment should be fully closed without any gas purging during the third step of the protocol.
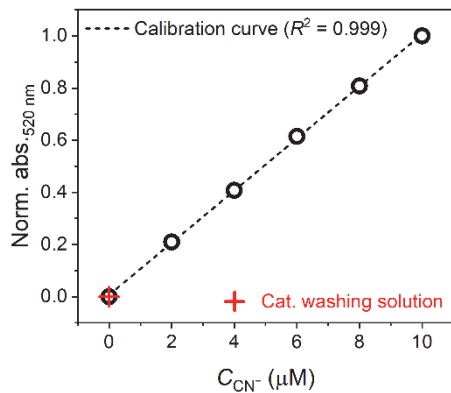
Figure S6. Determination of C_{CN^-} in rinsed water after the catalyst washing step using an UV-vis spectrophotometer at 520 nm.
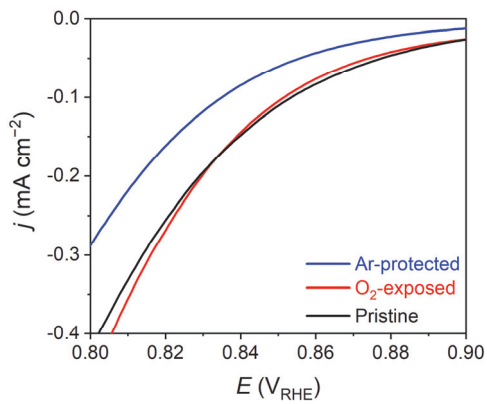
Figure S7. Effects of O_2 (or air) exposure during the *in situ* SD quantification protocol. ORR polarization curves of pristine and poisoned $Fe_{0.5}NC$ catalysts measured in O_2-saturated 0.1 M $HClO_4$ electrolyte. Cyanide poisoning experiment of $Fe_{0.5}NC$ was conducted using the original protocol (*i.e.*, E_{third} = 1.0 V_{RHE}, $C_{CN^-}^{electrolyte}$ = 200 μM, and electrolyte pH = 1) with and without Ar protection. The result shows that the O_2 (or air) exposure cannot effectively and irreversibly adsorb the cyanide probe on $Fe_{0.5}NC$, whereas a significant decrease in the ORR current is observed when the protocol is performed in an Ar-filled chamber. Hence, it is speculated that the interference induced by the competitive adsorption of O_2 is likely to significantly affect the extent of irreversible cyanide adsorption on $Fe_{0.5}NC$, owing to a very low cyanide concentration in the electrolyte during *in situ* SD quantification (*i.e.*, 200 μM). Therefore, O_2-free environment is essential for the accurate evaluation of SD.
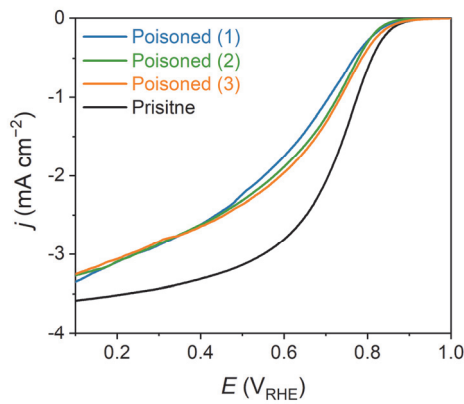
Figure S8. ORR polarization curves of pristine and poisoned $Fe_{0.5}NC$ measured in O_2-saturated 0.1 M $HClO_4$ electrolyte. Cyanide poisoning experiment of $Fe_{0.5}NC$ was conducted using the original *in situ* SD quantification protocol (*i.e.*, E_{third} = 1.0 V_{RHE}, $C_{CN^-}^{electrolyte}$ = 200 μM, and electrolyte pH = 1). ORR polarization curves were obtained by LSV in the potential range of 0.05–1.05 V_{RHE} at a scan rate of 10 mV s^{-1}. The results show a non-negligible deviation in the ORR activity of the poisoned $Fe_{0.5}NC$ in repeated measurements.
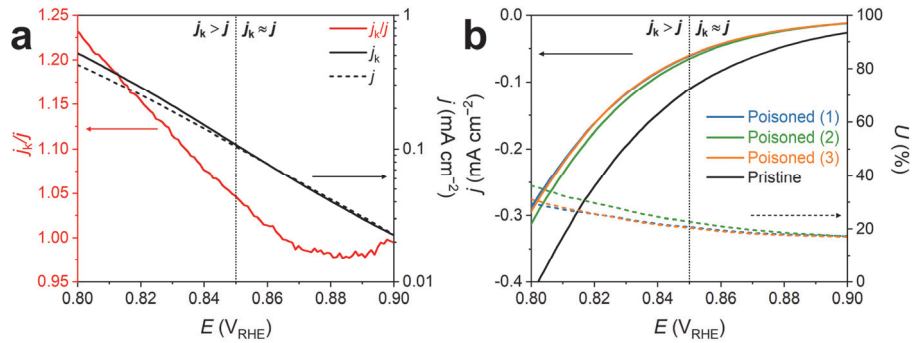
Figure S9. ORR measurement protocol after *in situ* SD quantification. (a) Measured j (black dashed line) and j_k (black solid line) derived with j_d of pristine $Fe_{0.5}NC$, and the ratio between them (j_k/j; red solid line). In the highly kinetic-controlled region (≥ 0.85 V_{RHE}), the measured j is almost comparable to j_k (*i.e.*, $j_k/j \approx 1$) without a considerable contribution of j_d. Therefore, the measured j at 0.85 V_{RHE} is directly used as the ORR activity term (*i.e.*, j_k) for *in situ* SD quantification. (b) ORR polarization curves of the pristine and poisoned $Fe_{0.5}NC$ measured in O_2-saturated 0.1 M $HClO_4$ electrolyte (solid line) and estimated U values as a function of potential (dashed line). Cyanide poisoning experiment of $Fe_{0.5}NC$ was performed using the original *in situ* SD quantification protocol (*i.e.*, $E_{third} = 1.0$ V_{RHE}, $C_{CN^-}^{electrolyte} = 200$ μM, and electrolyte pH = 1). Estimated U values are almost identical ($20 \pm 3\%$) at potentials above 0.85 V_{RHE}, while these gradually increase with further decrease in potential due to the non-negligible contribution of j_d to j (*i.e.*, $j_k/j \neq 1$).
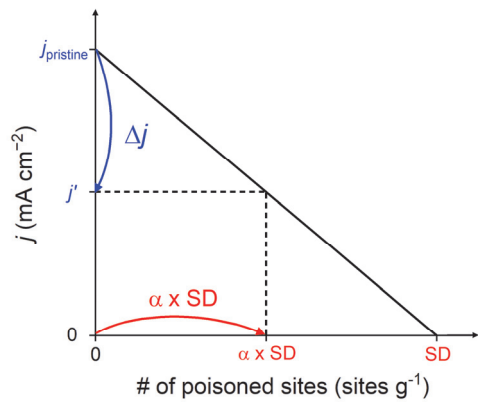
Figure S10. Linear correlation between the decrease in ORR activity (*i.e.*, Δj) and the amount of poisoned Fe-N$_x$ sites by cyanide (*i.e.*, $\alpha \times$ SD). The *j'* denotes the ORR activity of the cyanide-poisoned catalyst and the α denotes the SD ratio of the poisoned sites to the total sites of Fe-N$_x$ species.
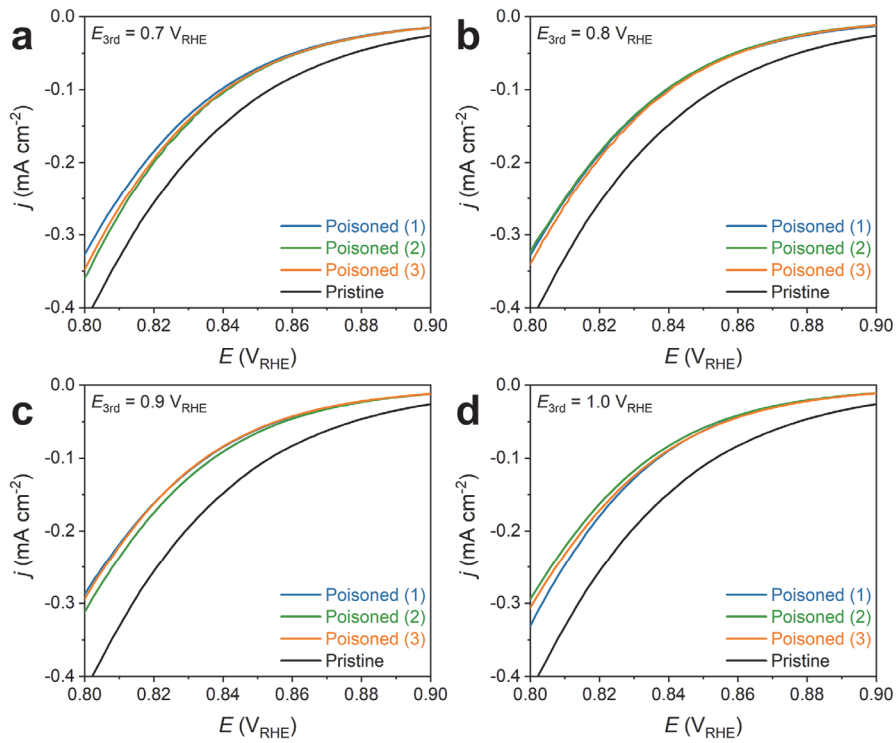
Figure S11. (a–d) ORR polarization curves of $Fe_{0.5}NC$ before and after *in situ* SD quantification with various E_{third} values of 0.7 (a), 0.8 (b), 0.9 (c), and 1.0 V_{RHE} (d). ORR activity was measured in O_2-saturated 0.1 M $HClO_4$ electrolyte. The initial $C_{CN^-}^{electrolyte}$ and electrolyte pH were fixed at 200 μM and 1, respectively.
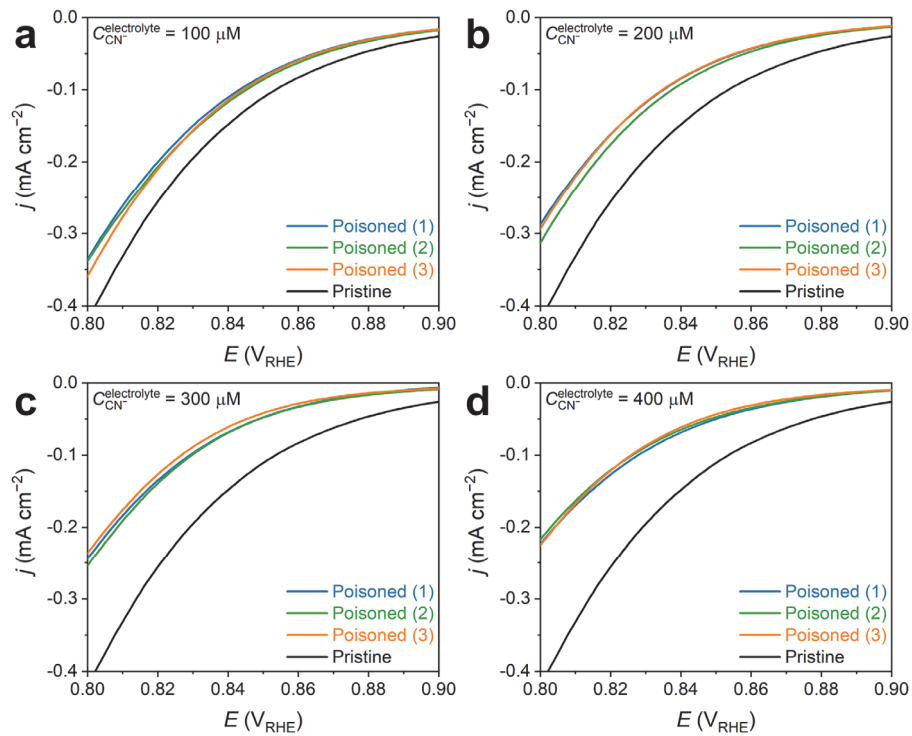
Figure S12. (a–d) ORR polarization curves of Fe$_{0.5}$NC before and after *in situ* SD quantification with various initial $C_{CN^-}^{electrolyte}$ values of 100 (a), 200 (b), 300 (c), and 400 μM (d). ORR activity was measured in O$_2$-saturated 0.1 M HClO$_4$ electrolyte. The E_{third} and electrolyte pH were fixed at 1.0 V$_{RHE}$ and 1, respectively.
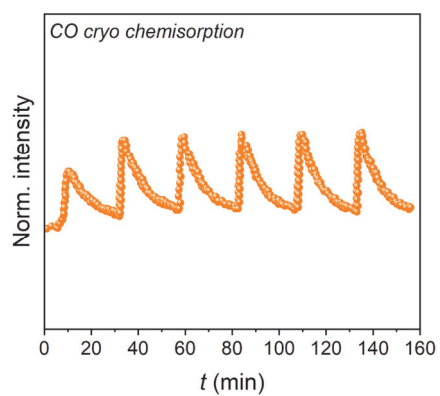
Figure S13. SD quantification of $Fe_{0.5}NC$ employing the CO uptake trajectory. Reproduced from *ACS Catal*. **2019**, *9* (6) 4841-4852.[6] Copyright [2019] American Chemical Society. Prior to CO adsorption, the sample was pre-treated at 873 K. This chemisorption method afforded a reliable SD value of $(3.80 \pm 0.21) \times 10^{19}$ sites g^{-1} (*i.e.*, U = *ca.* 23%).
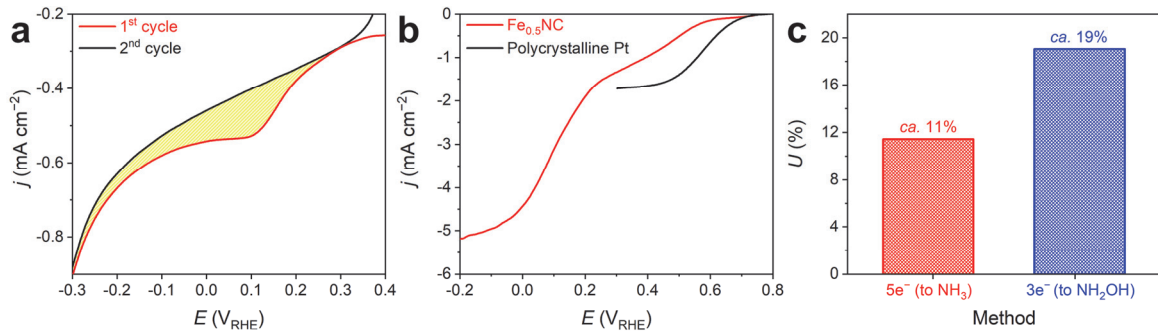
Figure S14. SD quantification of Fe$_{0.5}$NC using *in situ* NO$_2^-$-stripping voltammetry. (a) Reductive stripping voltammograms of nitrosyl-poisoned Fe$_{0.5}$NC. The voltammograms were acquired in Ar-saturated 0.5 M acetate buffer electrolyte (pH 5.2) at a scan rate of 10 mV s^{-1}. The yellow-colored area was integrated to calculate the U value. (b) NO reduction reaction (NORR) polarization curves of Fe$_{0.5}$NC and polycrystalline Pt electrode. NORR polarizations were investigated using a scan rate of 10 mV s^{-1} and rotation speed of 1600 rpm in NO-saturated 0.1 M HClO$_4$ electrolyte. (c) U values of Fe$_{0.5}$NC estimated from stripping results. It was assumed that reductive stripping converted the nitrosyl ligand either to NH$_3$ (five-electron transfer) or NH$_2$OH (three-electron transfer). Notably, five-electron transfer was employed for SD quantification in a previous Malko's report,[5] but in the present study, three-electron transfer to the nitrosyl ligand was assumed owing to the reason discussed below.

Additional discussion: For comparison, the SD of Fe$_{0.5}$NC was also estimated using the NO$_2^-$-stripping method developed by Malko *et al.*[5] This method is based on the reductive stripping of the nitrosyl ligand adsorbed onto the Fe-N$_x$ moieties, and the number of electrons transferred during nitrosyl ligand reduction (n) is one of the key variables for SD calculation. The authors first assumed that Fe-N-C catalyst mainly catalyzes the reduction of nitrosyl ligand (or NO) to NH$_3$ (five-electron transfer). However, it was observed that j_d for Fe$_{0.5}$NC was -5.2 mA cm^{-2} (Figure S14b), which was almost three times higher than that for polycrystalline Pt ($j_d = -1.7$ mA cm^{-2}), which mainly catalyzes the conversion of NO to N$_2$O (one-electron transfer).[16-18] This indicated that the main product from nitrosyl ligand (or NO) reduction on Fe$_{0.5}$NC was NH$_2$OH (*i.e.*, $n = 3$). As the experimental conditions for stripping and NORR were not identical (*i.e.*, electrolyte pH of 5.2 and 1, respectively), the n value for NO$_2^-$-stripping on Fe$_{0.5}$NC could not be explicitly defined. However, the experimentally determined U value of Fe$_{0.5}$NC assuming three-electron transfer (*ca.* 19%) was in good agreement with that estimated from the *in situ* SD quantification using a cyanide probe and CO chemisorption.[6] Assuming five-electron transfer, the estimated U value was only *ca.* 11%, which was significantly lower than those obtained using other methods.
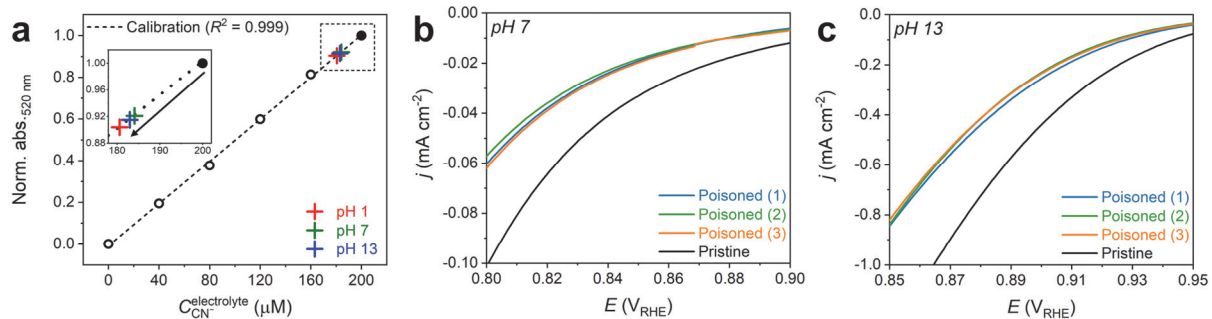
Figure S15. (a) Determination of $C_{CN^-}^{electrolyte}$ after the *in situ* SD quantification of Fe$_{0.5}$NC at different electrolyte pH values. Calibration values are indicated by open circles, and initial $C_{CN^-}^{electrolyte}$ is indicated by a filled circle. (b,c) ORR polarization curves of Fe$_{0.5}$NC before and after *in situ* SD quantification at electrolyte pH of 7 (b) and 13 (c). The E_{third} and $C_{CN^-}^{electrolyte}$ were fixed at 1.0 V$_{RHE}$ and 200 μM, respectively. The SD of Fe$_{0.5}$NC at pH 13 is calculated at 0.90 V$_{RHE}$ because of the high kinetic-controlled region in the alkaline medium.
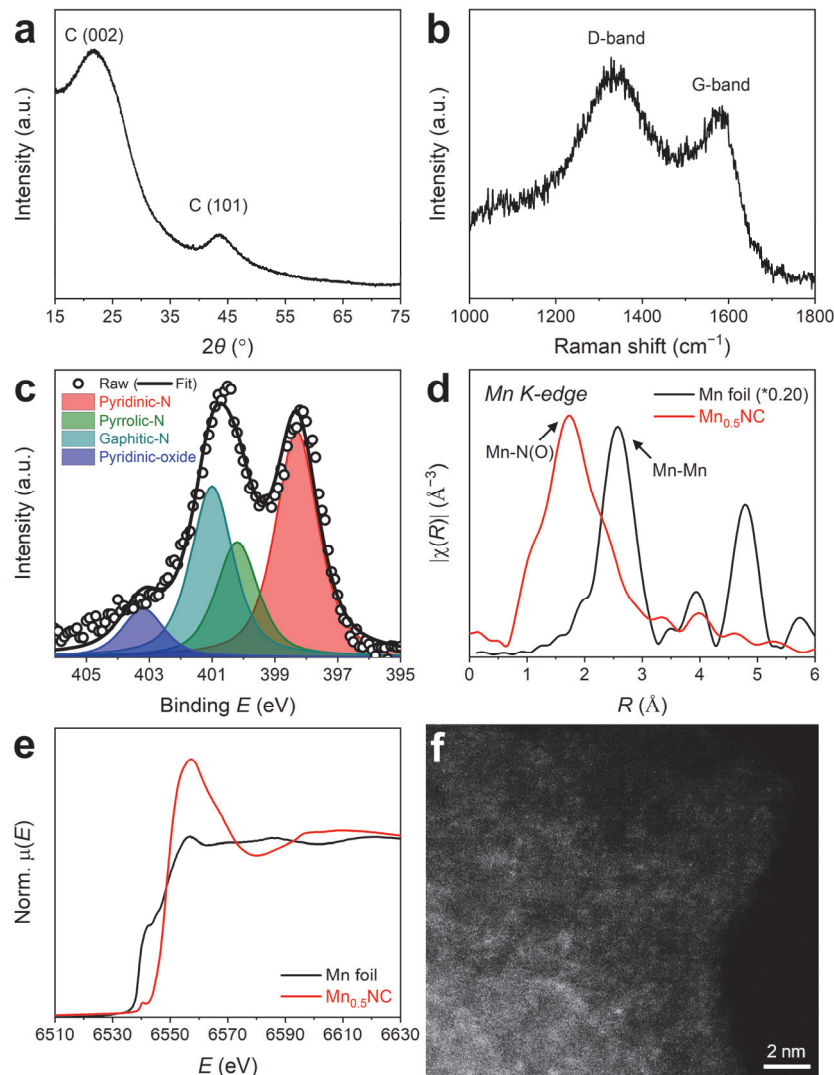
Figure S16. Physicochemical characterization of $Mn_{0.5}NC$. (a) XRD pattern and (b) Raman spectrum of $Mn_{0.5}NC$. Two main peaks of graphite in the XRD pattern and D-/G-band signals in the Raman spectrum reveal the successful carbonization of the $Mn_{0.5}NC$ precursor mixture during pyrolysis. (c) XPS-N_{1s} spectrum of $Mn_{0.5}NC$. The peaks are deconvoluted with four N-components: pyridinic-N (398.5 eV), pyrrolic-N (400.1 eV), graphitic-N (401.1 eV), and pyridinic-oxide (403.2 eV).[13] (d) Mn K-edge EXAFS and (e) XANES spectra of $Mn_{0.5}NC$. The EXAFS spectrum of $Mn_{0.5}NC$ shows a strong backscattering signal for Mn-N (or Mn-O) bonds without Mn-Mn interaction, indicating the predominant presence of single-atom Mn sites in $Mn_{0.5}NC$. (f) HAADF-STEM image of $Mn_{0.5}NC$ (scale bar = 2 nm).
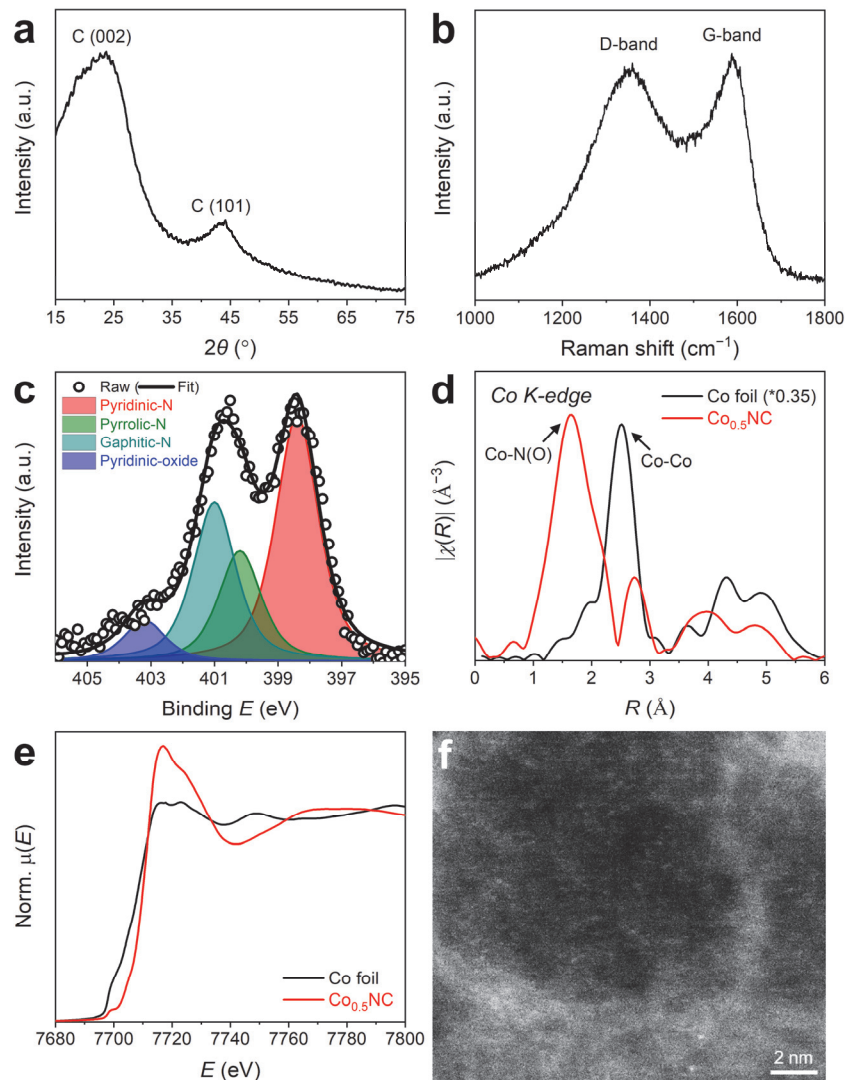
Figure S17. Physicochemical characterization of $Co_{0.5}NC$. (a) XRD pattern and (b) Raman spectrum of $Co_{0.5}NC$. Two main peaks of graphite in the XRD pattern and D-/G-band signals in the Raman spectrum reveal the successful carbonization of the $Co_{0.5}NC$ precursor mixture during pyrolysis. (c) XPS-N_{1s} spectrum of $Co_{0.5}NC$. The peaks are deconvoluted with four N-components: pyridinic-N (398.5 eV), pyrrolic-N (400.1 eV), graphitic-N (401.1 eV), and pyridinic-oxide (403.2 eV).[13] (d) Co K-edge EXAFS and (e) XANES spectra of $Co_{0.5}NC$. The EXAFS spectrum of $Co_{0.5}NC$ shows a strong backscattering signal for Co-N (or Co-O) bonds without Co-Co interaction, indicating the predominant presence of single-atom Co sites in $Co_{0.5}NC$. (f) HAADF-STEM image of $Co_{0.5}NC$ (scale bar = 2 nm).
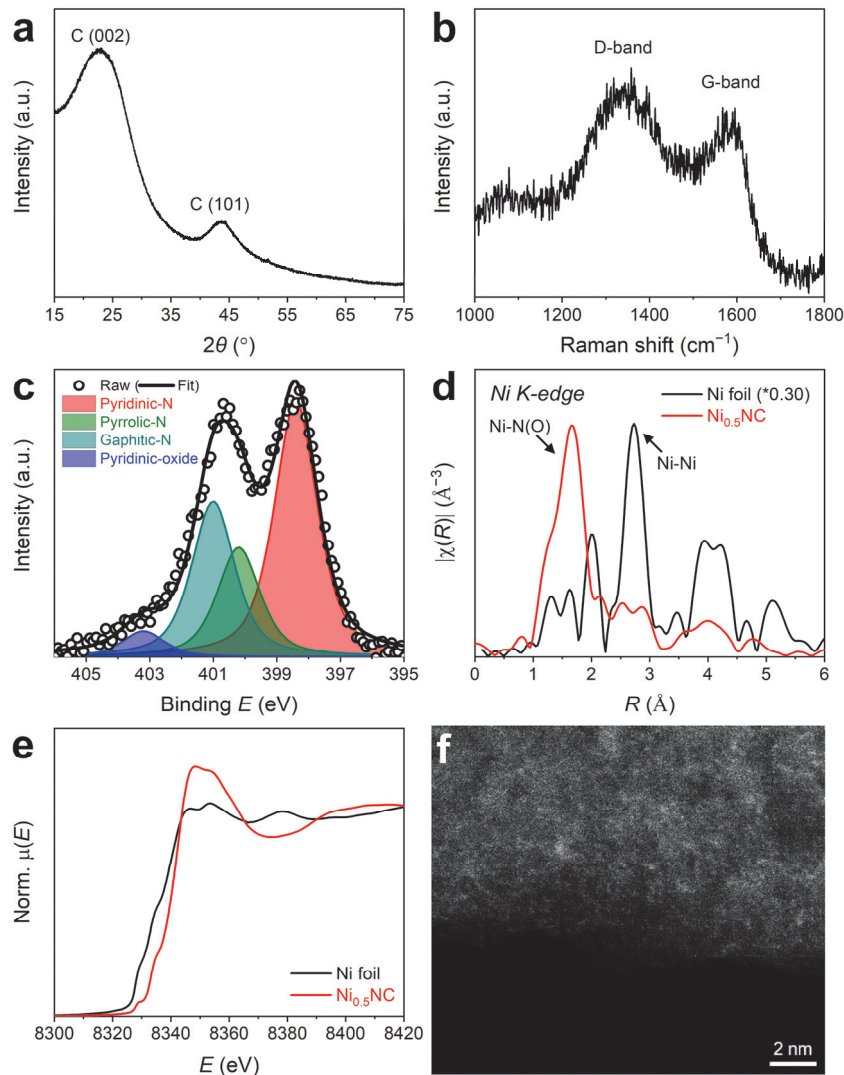
Figure S18. Physicochemical characterization of $Ni_{0.5}NC$. (a) XRD pattern and (b) Raman spectrum of $Ni_{0.5}NC$. Two main peaks of graphite in the XRD pattern and D-/G-band signals in the Raman spectrum reveal the successful carbonization of the $Ni_{0.5}NC$ precursor mixture during pyrolysis. (c) XPS-N_{1s} spectrum of $Ni_{0.5}NC$. The peaks are deconvoluted with four N-components: pyridinic-N (398.5 eV), pyrrolic-N (400.1 eV), graphitic-N (401.1 eV), and pyridinic-oxide (403.2 eV).[13] (d) Ni K-edge EXAFS and (e) XANES spectra of $Ni_{0.5}NC$. The EXAFS spectrum of $Ni_{0.5}NC$ shows a strong backscattering signal for Ni-N (or Ni-O) bonds without Ni-Ni interaction, indicating the predominant presence of single-atom Ni sites in $Ni_{0.5}NC$. (f) HAADF-STEM image of $Ni_{0.5}NC$ (scale bar = 2 nm).
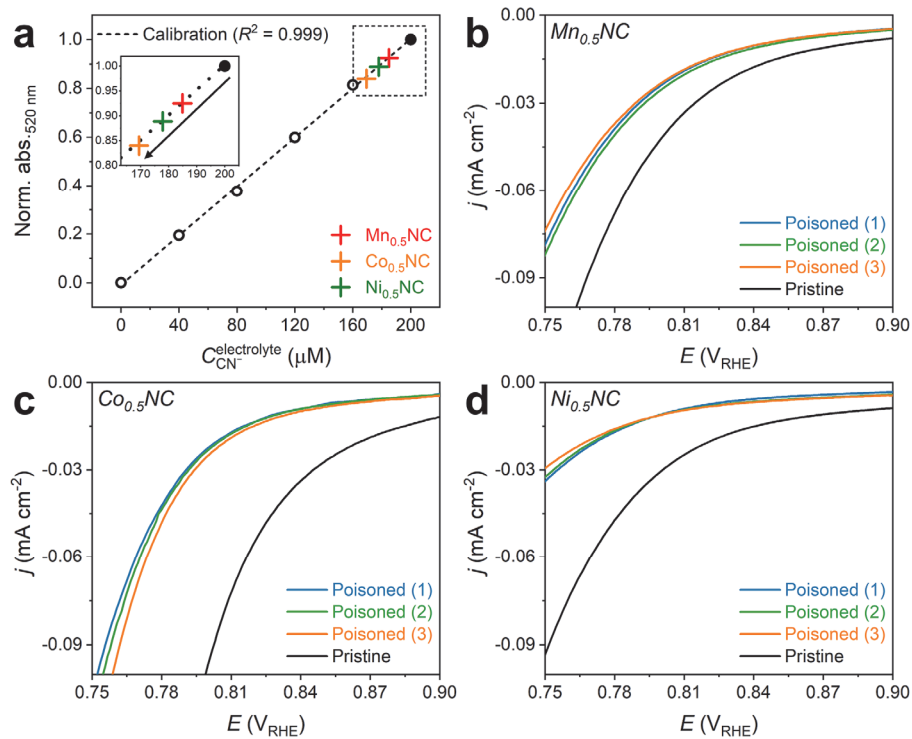
Figure S19. (a) Determination of $C_{CN^-}^{electrolyte}$ after the *in situ* SD quantification of Me$_{0.5}$NC catalysts (Me = Mn, Co, and Ni). Calibration values are indicated by open circles, and the initial $C_{CN^-}^{electrolyte}$ is indicated by a filled circle. (b–d) ORR polarization curves before and after the *in situ* SD quantification of Me$_{0.5}$NC catalysts; Mn$_{0.5}$NC (b), Co$_{0.5}$Nc (c), and Ni$_{0.5}$NC (d). ORR activity was measured in O$_2$-saturated 0.1 M HClO$_4$ electrolyte. The cyanide poisoning experiments of Me$_{0.5}$NC catalysts were conducted using the original *in situ* SD quantification protocol (*i.e.*, E_{third} = 1.0 V$_{RHE}$, $C_{CN^-}^{electrolyte}$ = 200 μM, and electrolyte pH = 1).
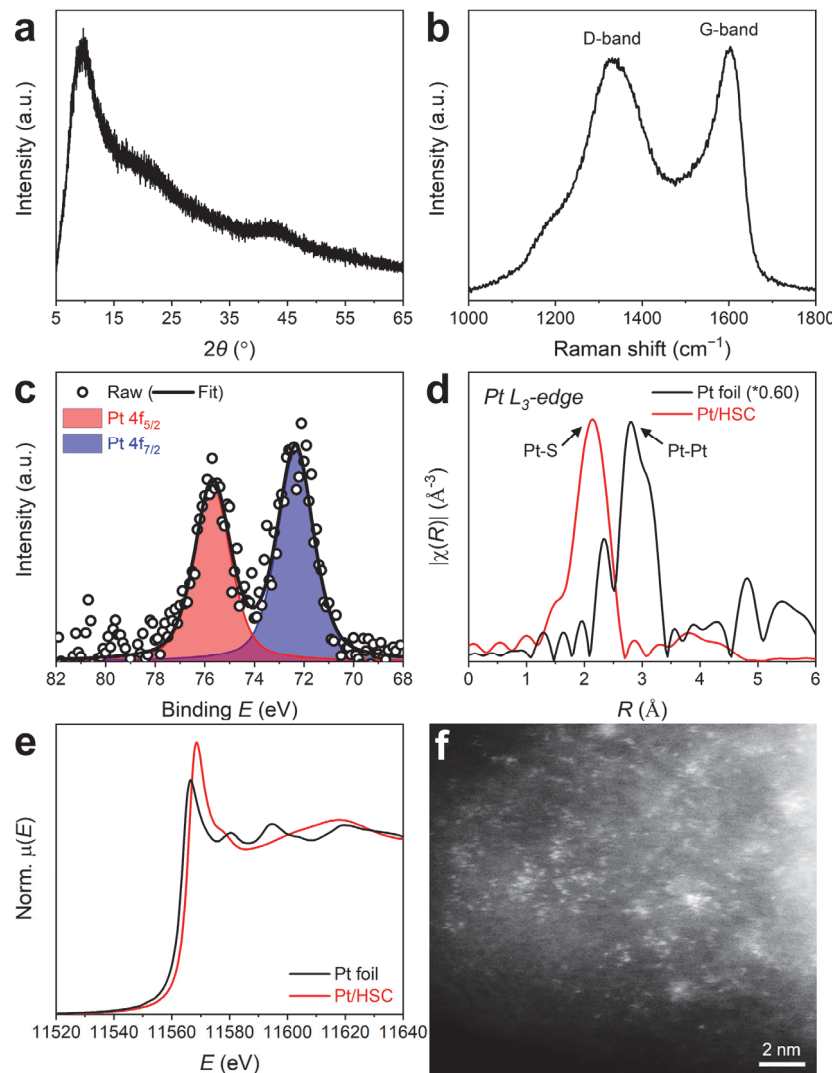
Figure S20. Physicochemical characterization of Pt/HSC. (a) XRD pattern, (b) Raman spectrum, and (c) XPS-Pt$_{4f}$ spectrum of Pt/HSC. The binding energy used for the peak deconvolution of the XPS-Pt spectra (for 4f$_{7/2}$) is 72.2 eV for Pt^{2+} and the spin-orbit splitting for 4f$_{5/2}$ and 4f$_{7/2}$ peaks is 3.33 eV.[19] (d) Pt L$_3$-edge EXAFS and (e) XANES spectra of Pt/HSC. The EXAFS spectrum of Pt/HSC shows a strong backscattering signal for Pt-S bonds without Pt-Pt interaction, indicating the predominant presence of single-atom Pt sites in Pt/HSC. A detailed discussion of Pt/HSC can be found in our previous work.[19] (f) HAADF-STEM image of Pt/HSC (scale bar = 2 nm).
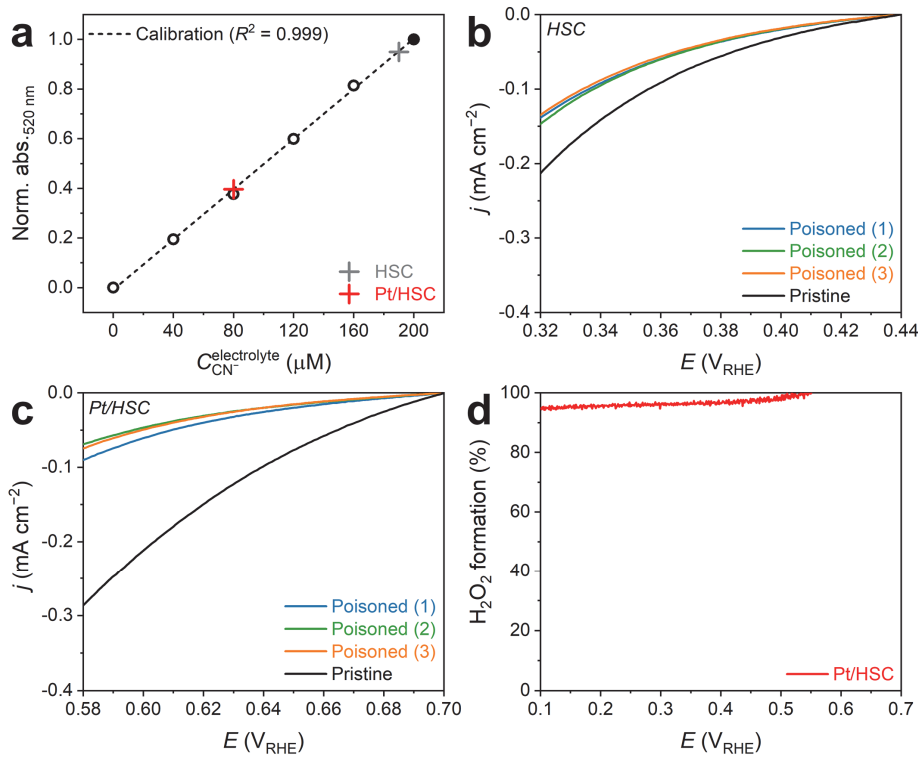
Figure S21. (a) Determination of $C_{CN^-}^{electrolyte}$ after the *in situ* SD quantification of HSC and Pt/HSC. Calibration values are indicated by open circles, and initial $C_{CN^-}^{electrolyte}$ is indicated by a filled circle. (b,c) ORR polarization curves before and after the *in situ* SD quantification of HSC (b) and Pt/HSC (c). ORR activity was measured in O_2-saturated 0.1 M $HClO_4$ electrolyte. The cyanide poisoning experiments of HSC and Pt/HSC were conducted using the original *in situ* SD quantification protocol (*i.e.*, E_{third} = 1.0 V_{RHE}, $C_{CN^-}^{electrolyte}$ = 200 μM, and electrolyte pH = 1). (d) H_2O_2 formation profile of Pt/HSC. The Pt ring, equipped at the rotating ring-disk electrode, was polarized at a constant potential of 1.2 V_{RHE} during ORR polarization on the disk electrode, and a collection efficiency of 0.43 was used after Fe^{2+}/Fe^{3+} redox calibration. Owing to the low ORR onset potentials of HSC and Pt/HSC compared to that of the $Me_{0.5}NC$ catalysts, their LSV curves were obtained in the potential range of 0.20–0.50 V_{RHE} for HSC and 0.45–0.75 V_{RHE} for Pt/HSC. The SD and TOF of Pt/HSC were calculated at 0.65 V_{RHE}.
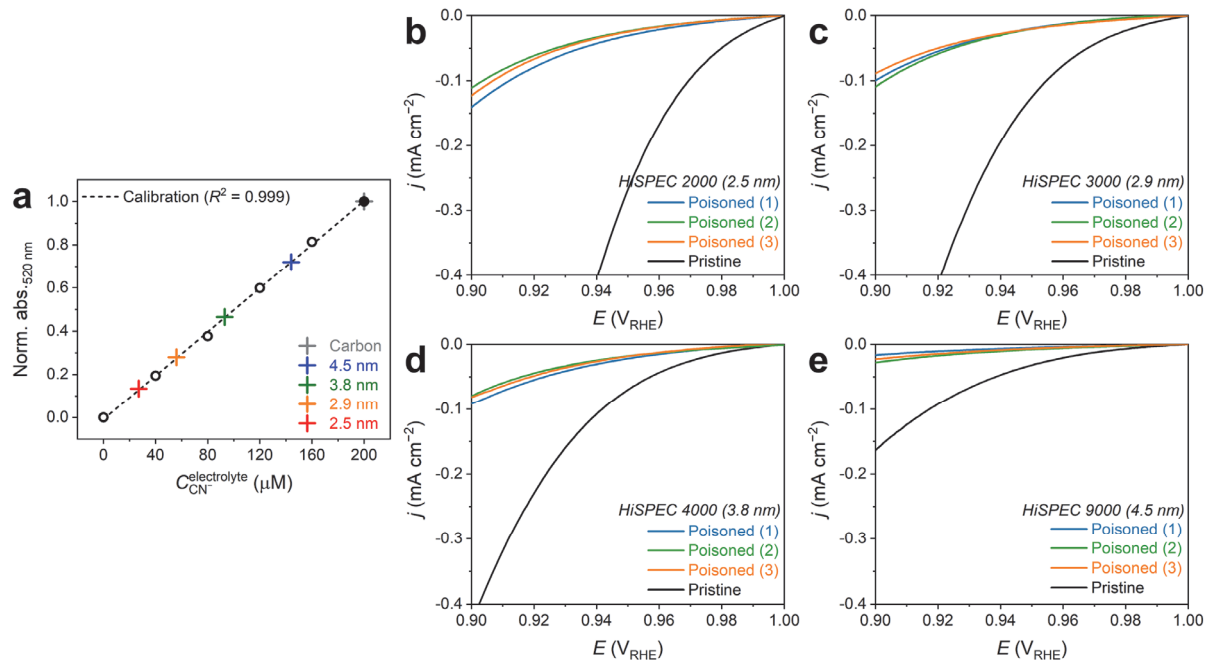
Figure S22. (a) Determination of $C_{CN^-}^{electrolyte}$ after the SD quantification of Pt nanoparticles with different particle sizes (*i.e.*, 2.5, 2.9, 3.8, and 4.5 nm). Calibration values are indicated by open circles, and initial $C_{CN^-}^{electrolyte}$ is indicated by a filled circle. (b–e) ORR polarization curves before and after the *in situ* SD quantification of Pt nanoparticles; HiSPEC 2000 (b), HiSPEC 3000 (c), HiSPEC 4000 (d), and HiSPEC 9000 (e). ORR activity was measured in O_2-saturated 0.1 M $HClO_4$ electrolyte. The cyanide poisoning experiments of Pt nanoparticles were conducted using the original *in situ* SD quantification protocol (*i.e.*, $C_{CN^-}^{electrolyte}$ = 200 μM and electrolyte pH = 1) except for E_{third} = 0.6 V_{RHE} to prevent surface oxide formation of Pt nanoparticles.
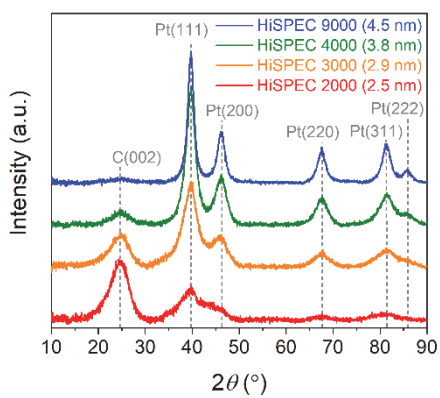
Figure S23. XRD patterns of Pt nanoparticle catalysts having different particle sizes (2.5–4.5 nm). The peaks were assigned to (111), (200), (220), (311), and (222) planes of face-centered cubic (fcc) Pt.[20] The peaks become sharpened as the crystalline size increases.
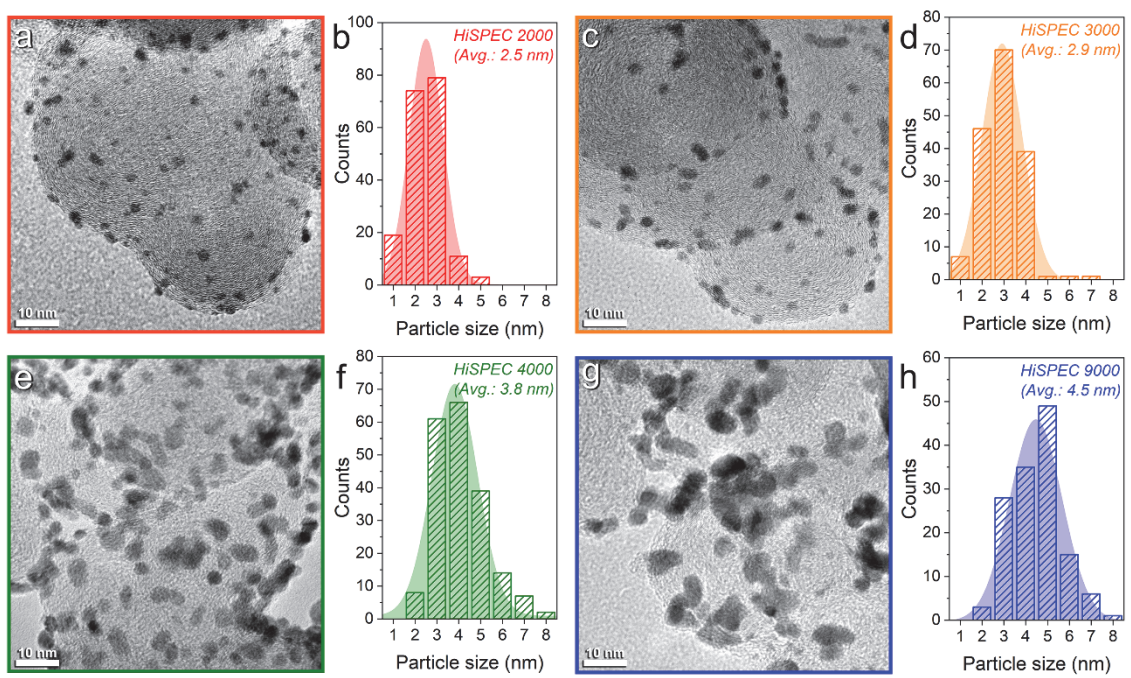
Figure S24. (a–h) TEM images and histograms of the particle size distribution of HiSPEC 2000 (a,b), HiSPEC 3000 (c,d), HiSPEC 4000 (e,f), and HiSPEC 9000 (g,h). The results showed that average Pt particle sizes were 2.5, 2.9, 3.8, and 4.5 nm for commercial HiSPEC 2000, HiSPEC 3000, HiSPEC 4000, and HiSPEC 9000 catalysts, respectively.
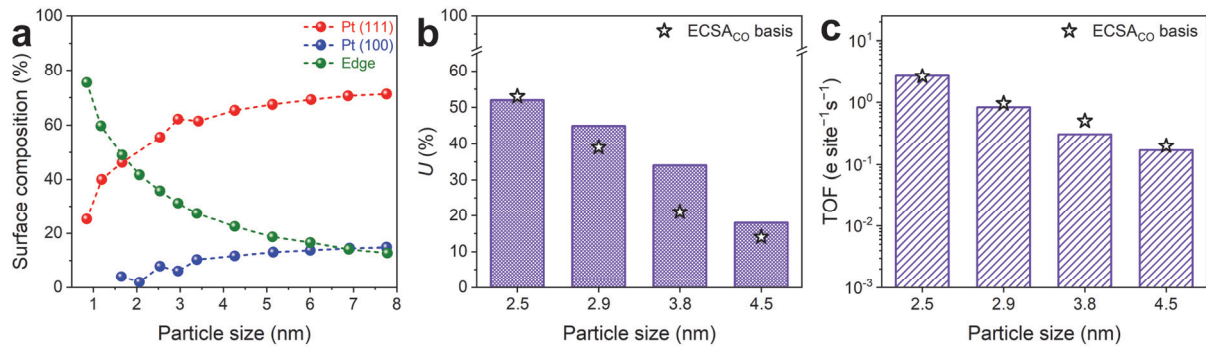
Figure S25. (a) Particle-size-dependent surface compositions of Pt(111), Pt(100), and edge sites, estimated based on the DFT calculations with truncated octahedral-shaped model nanoparticles. Reproduced from *Nano Lett.* **2011**, *11* (9) 3714-3719.[11] Copyright [2011] American Chemical Society. (b,c) Estimated U (b) and TOF (c) values of Pt nanoparticles with different particle sizes (2.5–4.5 nm). In this estimation, the contributions of Pt(111), Pt(100), and edge sites to cyanide adsorption were considered, and it was assumed that their surface coverages (*i.e.*, CN$^-$/Pt) were 0.5, 1.0, and 1.0, respectively. The U and TOF values obtained by ECSA$_{CO}$ are indicated by star symbols for comparison.

Table S1. The metal content in the $Me_{0.5}NC$ catalysts obtained from ICP-AES.

Sample	$Fe_{0.5}NC$	$Mn_{0.5}NC$	$Co_{0.5}NC$	$Ni_{0.5}NC$
Metal content (wt %)	1.5	1.4	1.4	1.5

Table S2. Parameters derived from the fittings of the Mössbauer spectrum of $Fe_{0.5}NC$: relative area (RA), isomer shift (IS), and quadrupole splitting (QS) of each fitted spectral component.

Sample	Component	RA (%)	IS (mm s^{-1})	QS (mm s^{-1})	Assignment
Fe$_{0.5}$NC powder	D1	59	0.33	0.88	High spin O-Fe^{3+}-N$_4$
	D2	41	0.37	2.73	Low/medium spin Fe^{2+}-N$_4$

Table S3. Physical properties of commercial Pt nanoparticles provided by a manufacture.[21]

Catalyst	Product	Pt content (wt%)	Metal surface area ($m^2\ g^{-1}$)	XRD crystalline size (nm)
HiSPEC 2000	Pt / XC72R	9.5–10.5	105 (min.)	3.0 (max.)
HiSPEC 3000	Pt / XC72R	19.0–21.0	90 (min.)	3.5 (max.)
HiSPEC 4000	Pt / XC72R	38.0–41.0	60 (min.)	4.5 (max.)
HiSPEC 9000	Pt / XC72R	56.0–60.0	40 (min.)	5.0 (max.)

Supplementary Note 5

Laboratory safety guidelines: Safety is the most important factor in laboratory work. Please read the instructions and precautions thoroughly and follow the laboratory safety guidelines for the operator's health if performing identical or modified experiments elsewhere.

Acute Toxic   Health Hazard   Flammable   Environmental Hazard

Hazards: Inhalation, absorption, and swallowing of cyanides and hydrogen cyanide are fatal to human health.[22,23] Swallowing 5 μg $kg^{-1}_{Body\ weight}$ of KCN or inhalation of 143 ppm HCN for 60 min causes the death of one-half of a group of rats.[24] Low levels of exposure to these toxic substances can cause signs and symptoms within a few minutes, including irritation, headache, confusion, dizziness, rapid breathing, nausea, and vomiting.

Precautions: Never perform the experiments alone when using cyanide. All experiments should always be conducted under the supervision of the director or another lab member who can immediately assist in the event of a cyanide emergency. Use appropriate personal protective equipment (PPE), *e*.g., lab coat, eye protection, chemical-resistant gloves, etc. During the entire procedure, the operators should be separated from the cyanide sources using appropriate equipment, such as a glovebox and a fume hood. An operator must be equipped with an HCN detector during the experiments to avoid the inhalation of HCN (Figure S26).
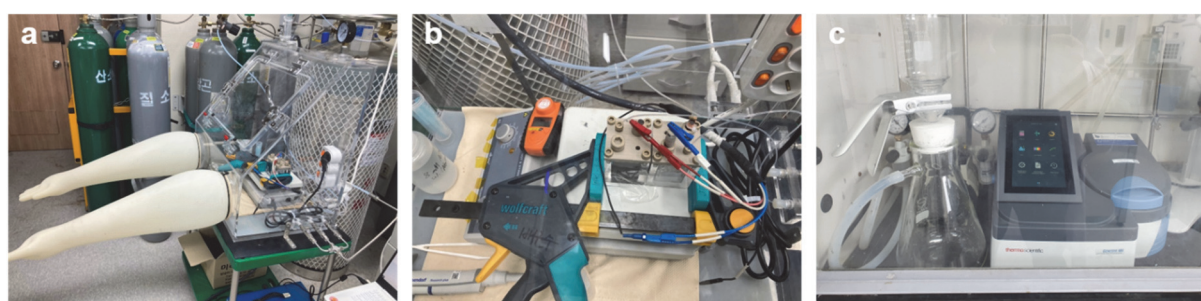
Figure S26. Experimental setup for ensuring safety during the *in situ* SD quantification with cyanide. (a) Lab-made glovebox filled with Ar gas (which equips gas-inlet/outlet lines), (b) electrochemical cell and other equipment placed in the glove box, and (c) vacuum pump and UV-vis spectrophotometer placed in the fume hood.

Emergency procedures

[1. Cyanide poisoning] First, seek immediate medical attention and treatment. This procedure gives first aid instructions for victims. 1) Inhalation: Immediately move the victim to a fresh air environment if the victim inhales cyanide. 2) Ingestion: Do not induce vomiting, and monitor the victim's respiration. 3) Absorption: Remove cyanide sources from the victim immediately. Wash the victim's exposed skin vigorously with a large quantity of water/soap to prevent cyanide's adsorption through the victim's skin.

[2. Cyanide spills/leaks] Do not attempt to clean up large spills. Evacuate the laboratory and post a "Do not enter" sign on the laboratory entrance until the appropriate experts clear the laboratory/building. In the case of a small spill, clean up liquid using sand or an inert absorbent and remove it to a safe place. Cautiously neutralize with oxidants such as hypochlorite and hydrogen peroxide, followed by washing with plenty of water.[25]

For more detailed emergency procedures, please refer to the Emergency Response Safety and Health Database of the National Institute for Occupational Safety and Health (NIOSH).

References

1.	Mineva, T.; Matanovic, I.; Atanassov, P.; Sougrati, M.-T.; Stievano, L.; Clémancey, M.; Kochem, A.; Latour, J.-M.; Jaouen, F., Understanding Active Sites in Pyrolyzed Fe–N–C Catalysts for Fuel Cell Cathodes by Bridging Density Functional Theory Calculations and [57]Fe Mössbauer Spectroscopy. *ACS Catal.* **2019,** *9* (10), 9359-9371.

2.	Kocha, S. S.; Shinozaki, K.; Zack, J. W.; Myers, D. J.; Kariuki, N. N.; Nowicki, T.; Stamenkovic, V.; Kang, Y.; Li, D.; Papageorgopoulos, D., Best Practices and Testing Protocols for Benchmarking ORR Activities of Fuel Cell Electrocatalysts Using Rotating Disk Electrode. *Electrocatalysis* **2017,** *8* (4), 366-374.

3.	Yeddou, A. R.; Nadjemi, B.; Halet, F.; Ould-Dris, A.; Capart, R., Removal of Cyanide in Aqueous Solution by Oxidation with Hydrogen Peroxide in Presence of Activated Carbon Prepared From Olive Stones. *Miner. Eng.* **2010,** *23* (1), 32-39.

4.	Teixeira, L. A. C.; Arellano, M. T. C.; Marquez Sarmiento, C.; Yokoyama, L.; Araujo, F. V. d. F., Oxidation of Cyanide in Water by Singlet Oxygen Generated by the Reaction Between Hydrogen Peroxide and Hypochlorite. *Miner. Eng.* **2013,** *50-51*, 57-63.

5.	Malko, D.; Kucernak, A.; Lopes, T., *In situ* Electrochemical Quantification of Active Sites in Fe–N/C Non-Precious Metal Catalysts. *Nat. Commun.* **2016,** *7* (1), 13285.

6.	Luo, F.; Choi, C. H.; Primbs, M. J. M.; Ju, W.; Li, S.; Leonard, N. D.; Thomas, A.; Jaouen, F.; Strasser, P., Accurate Evaluation of Active-Site Density (SD) and Turnover Frequency (TOF) of PGM-Free Metal–Nitrogen-Doped Carbon (MNC) Electrocatalysts using CO cryo Adsorption. *ACS Catal.* **2019,** *9* (6), 4841-4852.

7.	Chen, D.; Li, Y.; Liao, S.; Su, D.; Song, H.; Li, Y.; Yang, L.; Li, C., Ultra-High-Performance Core–Shell Structured Ru@Pt/C Catalyst Prepared by a Facile Pulse Electrochemical Deposition Method. *Sci. Rep.* **2015,** *5* (1), 11604.

8.	Shao, M. H.; Sasaki, K.; Liu, P.; Adzic, R. R., Pd₃Fe and Pt Monolayer-Modified Pd₃Fe Electrocatalysts for Oxygen Reduction. *Z. Phys. Chem.* **2007,** *221* (9-10), 1175-1190.

9.	Li, J.; Sougrati, M. T.; Zitolo, A.; Ablett, J. M.; Oğuz, I. C.; Mineva, T.; Matanovic, I.; Atanassov, P.; Huang, Y.; Zenyuk, I.; Di Cicco, A.; Kumar, K.; Dubau, L.; Maillard, F.; Dražić, G.; Jaouen, F., Identification of Durable and Non-Durable FeNₓ Sites in Fe–N–C Materials for Proton Exchange Membrane Fuel Cells. *Nat. Catal.* **2021,** *4* (1), 10-19.

10.	Ren, B.; Wu, D.-Y.; Mao, B.-W.; Tian, Z.-Q., Surface-Enhanced Raman Study of Cyanide Adsorption at the Platinum Surface. *J. Phys. Chem. B* **2003,** *107* (12), 2752-2758.

11.	Shao, M.; Peles, A.; Shoemaker, K., Electrocatalysis on Platinum Nanoparticles: Particle Size Effect on Oxygen Reduction Reaction Activity. *Nano Lett.* **2011,** *11* (9), 3714-3719.

12.	Stuhlmann, C.; Villegas, I.; Weaver, M. J., Scanning Tunneling Microscopy and Infrared Spectroscopy as Combined In Situ Probes of Electrochemical Adlayer Structure. Cyanide on Pt(111). *Chem. Phys. Lett.* **1994,** *219* (3), 319-324.

13.	Guo, D.; Shibuya, R.; Akiba, C.; Saji, S.; Kondo, T.; Nakamura, J., Active Sites of Nitrogen-Doped Carbon Materials for Oxygen Reduction Reaction Clarified Using Model Catalysts. *Science* **2016,** *351* (6271), 361.

14.	Pitschmann, V.; Kobliha, Z.; Tušarová, I., A Simple Spectrophotometric Determination of Cyanides by

p-Nitrobenzaldehyde and Tetrazolium Blue. *Adv. Mil. Technol.* **2011,** *6*, 19-27.

15.   Guilbault, G. G.; Kramer, D. N., Ultra Sensitive, Specific Method for Cyanide Using *p*-Nitrobenzaldehyde and *o*-Dinitrobenzene. *Anal. Chem.* **1966,** *38* (7), 834-836.

16.   de Groot, M. T.; Merkx, M.; Wonders, A. H.; Koper, M. T. M., Electrochemical Reduction of NO by Hemin Adsorbed at Pyrolitic Graphite. *J. Am. Chem. Soc.* **2005,** *127* (20), 7579-7586.

17.   de Groot, M. T.; Merkx, M.; Koper, M. T. M., Heme Release in Myoglobin−DDAB Films and Its Role in Electrochemical NO Reduction. *J. Am. Chem. Soc.* **2005,** *127* (46), 16224-16232.

18.   de Vooys, A. C. A.; Koper, M. T. M.; van Santen, R. A.; van Veen, J. A. R., Mechanistic Study of the Nitric Oxide Reduction on a Polycrystalline Platinum Electrode. *Electrochim. Acta* **2001,** *46* (6), 923-930.

19.   Choi, C. H.; Kim, M.; Kwon, H. C.; Cho, S. J.; Yun, S.; Kim, H.-T.; Mayrhofer, K. J. J.; Kim, H.; Choi, M., Tuning Selectivity of Electrochemical Reactions by Atomically Dispersed Platinum Catalyst. *Nat. Commun.* **2016,** *7* (1), 10922.

20.   Hu, S.; Tian, M.; Ribeiro, E. L.; Duscher, G.; Mukherjee, D., Tandem Laser Ablation Synthesis in Solution-Galvanic Replacement Reaction (LASiS-GRR) for the Production of PtCo Nanoalloys as Oxygen Reduction Electrocatalysts. *J. Power Sources* **2016,** *306*, 413-423.

21.   Scientific, F. Lab Equipment and Lab Supplies. https://www.fishersci.com/us/en/home.html (accessed Nov 11, 2020).

22.   *Hydrogen cyanide*, CAS RN 74-90-8; rev. 1; New Jersey Department of Health: Trenton, NJ, **2011**.

23.   *Potassium cyanide*, CAS RN 151-50-8; rev. 11; Thermo Fisher Scientific: Fair Lawn, NJ, **2021**.

24.   Simeonova, F. P.; Fishbein, L., *Hydrogen Cyanide and Cyanides: Human Health Aspects*. World Health Organization: Geneva, Switzerland, **2004**; p 71.

25.   Young, C.; Jordan, T. S. Cyanide Remediation: Current and Past Techonologies, In *Proceedings of the 10th Annual Conference on Hazardous Waste Research*, Kansas State University, Manhattan, Kansas, May 23-24, **1995**; Erickson, L. E.; Tillison, D. L.; Grant, S. C.; McDonald, J. P., Eds.; pp 104-129.